



# Spectroscopic diagnosis of plasma generated from platinum metal using the optical emission method

Tuqa A. Khalepha<sup>1</sup> · Nisreen Kh. Abdalameer<sup>1</sup>

Received: 19 December 2023 / Accepted: 13 January 2024  
© The Author(s), under exclusive licence to The Optical Society of India 2024

**Abstract** This work gives a spectroscopic investigation that aims to diagnose the plasma created from a pure platinum target using the optical emission approach. The inquiry explores the distinctive attributes of the generated optical signals, providing a clear understanding of the plasma's composition and behavior. The laser emitted pulses lasting 10 ns, with a frequency of 8 Hz. As a result, the energy outputs obtained were 250 and 500 (mJ) at wavelengths of 1064 and 532 (nm), respectively. The laser was focused onto the target material, which was composed entirely of platinum, to create a precise beam focus. The target material was placed in an ambient atmosphere at normal atmospheric pressure conditions. The electron temperature was determined with the Boltzmann plot methodology. The electron density ( $n_e$ ) was estimated by analyzing the Stark broadening profile concurrently. The findings enhance our comprehension of plasma dynamics, perhaps leading to breakthroughs in materials science and plasma technology. This discovery represents a crucial advancement in utilizing optical emission spectroscopy for thorough plasma diagnostics and creates opportunities for additional research in related areas.

**Keywords** Boltzmann plot · Stark broadening · Pt · OEM

## Introduction

The optical emission method is a spectroscopic technique employed to examine the elemental composition of a

sample by analyzing the light released from the substance when it is stimulated or energized. Regarding your abstract on the spectroscopic diagnostic of plasma created from a pure platinum target, it is probable that the optical emission method is utilized to analyze the plasma's features by studying the light it produces. Laser-induced breakdown spectroscopy (LIBS) is a very adaptable method used for the examination and quantification of various substances. It relies on the optical identification of specific atomic and molecular components by observing the emission signals emitted from plasma generated by laser-induced processes [1]. The approach under consideration is characterized by its relative simplicity in comparison to many other elemental analysis methods. This attribute may be attributed to its uncomplicated experimental setup. The experimental setup involves the use of a pulsed laser to induce microplasma formation on the surface of interest [2, 3]. Subsequently, the elemental composition is determined by analyzing the emitted radiation from the plasma plume [4]. The characteristics and behavior of laser-induced plasma are influenced by multiple parameters, including the wavelength of the laser, the dimensions of the laser spot, and the temporal length of the laser pulse. The surrounding environment and other relevant parameters. Experiments may be conducted under two conditions: atmospheric pressure or in the presence of an ambient gas, using this particular approach [4–6]. The ablation process entails the use of laser energy to disperse throughout the sample via heat conduction, leading to the fusion and vaporization of the target material. As a result, a plasma plume is generated. One significant advantage of using this technology is its capacity to provide a direct chemical analysis of the substance without requiring any further preparation [7]. The ablation method, which involves the use of lasers with pulse lengths exceeding 1 ns, may be divided into three separate phases. In the first phase, the

✉ Nisreen Kh. Abdalameer  
nisreenka\_phys@csu.uobaghdad.edu.iq

<sup>1</sup> Department of Physics, College of Science for Women, University of Baghdad, Baghdad, Iraq

laser beam engages with the solid material, resulting in the fast ionization of the target's surface. The ionization process takes place within a temporal duration that is less than the temporal extent of the laser pulse [8]. In the subsequent phase, the plasma, leading to an isothermal expansion, efficiently absorbs the laser. During the third stage, after the cessation of the laser pulse, the plasma plume that emerges experiences a quasi-adiabatic expansion inside a medium [9]. The medium under consideration may include either a state of vacuum or a background gas, and its composition may or may not involve the existence of externally imposed fields. The given input comprises numerical values [10, 11]. In this study, we offer an investigation into the emission characteristics of plasma produced on the surface of platinum by the use of an Nd:YAG laser. Furthermore, a study was conducted to investigate the impact of different laser energy levels and wavelengths on the temperature and electron density of the ablated plasma plume of the Pt target. After the sample has been prepared and placed into the system, the next important step is to use optical fibers to transport light to the spectrometer. The optical fibers function as channels to transmit the gathered signals or produced light from the sample to the spectrometer for thorough examination. The optical fibers are crucial for maintaining the signal integrity during transmission, which is essential for accurate and reliable spectroscopic observations.

### Preparation the sample

The focus of this experimental investigation was the analysis of a sample consisting solely of platinum (Pt), with a mass percentage of 100%. A hydraulic press machine was employed to create a pellet measuring 10 mm in diameter and 4 mm in thickness, with a load of 10 tons for a duration of 15 min. The pellet was formed from a small quantity of material.

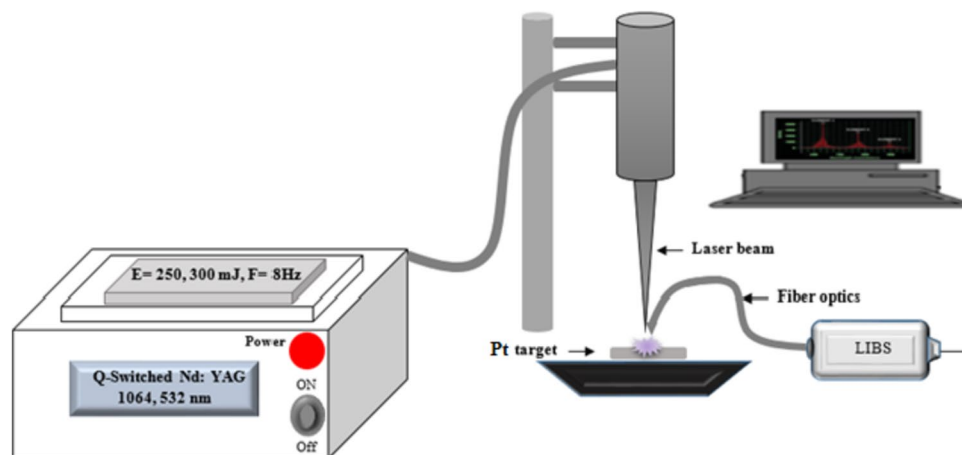
### Experimental setup

The experimental configuration is shown in Fig. 1. Experiments have been done under standard ambient conditions, namely at room temperature and atmospheric pressure. The plasma is generated by using pulses emitted from the Nd:YAG nanosecond laser, namely the 1064 FHG and 532 SHG wavelengths. These pulses possess an energy of 250 and 500 mJ, a pulse duration of 10 ns, and a repetition frequency of 8 Hz, when spot size 1.2 mm. The subject of interest in this study was platinum, which exhibited a high level of purity, with a concentration of around 99.999%. The laser beam is directed onto the surface of a platinum pallet that is present in the air at atmospheric pressure. This is achieved by using a quartz lens with a focal length of 10 cm. The optical emission light was acquired and examined using a Surwit (S3000-UV-NIR) spectrometer, using an optic fiber bundle with a core diameter of 50  $\mu\text{m}$ . The fiber was positioned at a distance of 1 cm. The plasma properties were estimated by using the NIST database software [12] to measure the optical emission line outcomes of certain components.

### Results and discussion

The breakdown encompasses a range of events, including surface sample heating accompanied by phase change and photoelectric emissions, as well as the presence of thermal ions and neutral plasma molecules. The evolution of laser-induced plasma encompasses a series of sequential processes. Initially, the emission of steady bremsstrahlung radiation takes place, followed by the subsequent expansion and cooling of the plasma. The detection of emissions of spectral lines occurring between closely linked energy levels is possible during the subsequent relaxing of the plasma. Following the production of plasma, these lines are observed to be embedded within a stream of

**Fig. 1** Block diagram of the experimental setup of the LIBS system



continuous emissions. Hence, the phenomenon of complete plasma radiation is observed initially as a continuous spectrum and comprises electronically excited pieces that undergo spontaneous decay, namely ions, atoms, and tiny molecules [13]. The plasma emissions were collected and subjected to analysis using an optical fiber bundle, which was then combined with a spectrometer. The spectrum peak intensities of the Cd plasma plume, caused by an Nd:YAG nanosecond laser, are depicted in Fig. 2a and b. The laser was operated within the energy of 250 and 500 mJ and emitted at two different wavelengths: the first harmonic at 1064 nm and the second harmonic at 532 nm. The relationship between laser energy and the observed intensity and width of spectral lines has been noted to be positive, indicating that as laser energy increases, both the intensity and width of the spectral lines also rise.

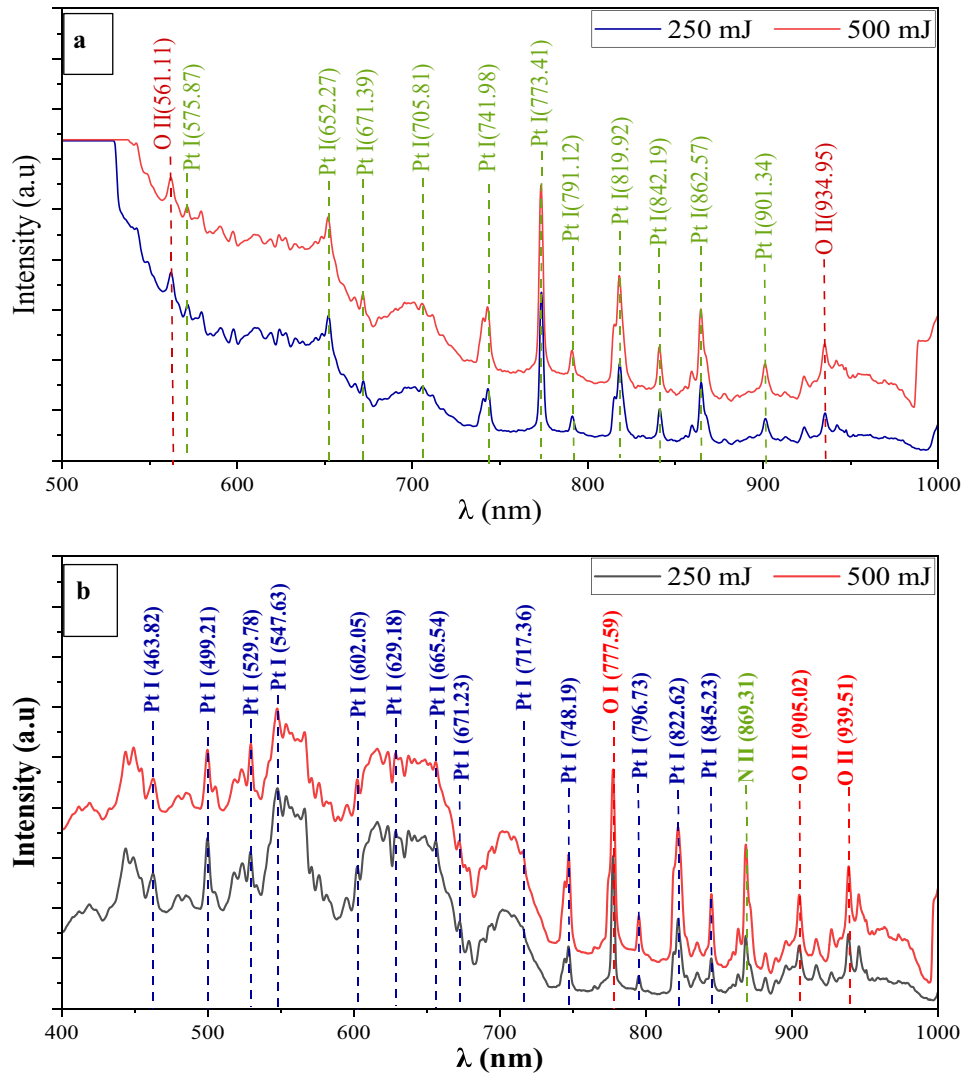
### Plasma temperature

Studies of laser-induced plasma emitted spectra help estimate the essential plasma parameters (i.e.,  $T_e$  and  $n_e$ ). In addition, the concept of the plasma characteristics depended on the electron temperature and described the relative distribution of the population by the Boltzmann law of the atoms over their energy level [6]. The Boltzmann plot method determined the plasma electron temperature based on the intensity of the observed spectral line. The plasma temperature equation can be written as in Eq. (1) [14] due to the predicted local thermodynamic equilibrium:

$$\ln\left(\frac{I_{ji}\lambda_{ji}}{A_{ji}g_{ji}}\right) = \frac{E_j}{k_B T_e} + C \quad (1)$$

Here, line identification and various spectroscopic parameters, including wavelength ( $\lambda_j$ ), statistical weight ( $g_j$ ), probability of transition ( $A_{ji}$ ), and upper energy ( $E_j$ ),

**Fig. 2** The emission spectra of platinum plasma inside a distinct window, encompassing the spectral ranges of 400 to 1000 nm. These spectra are generated by the utilization of the **a** 532 nm and **b** 1064 nm of the laser for different laser energy



obtained from a standard spectrum of the NIST database [10] and listed in Table 1,  $i$  and  $j$  refer to the low and upper level, respectively. ( $k_B$ ) is the Boltzmann constant,  $T_e$  is the plasma temperature, and  $C$  is the constant. To draw the Boltzmann plot, we used the atomic platinum Pt (I) lines

to deduce the plasma electron temperature, as shown in Fig. 3 of 1064 nm and Fig. 4 of 532 nm laser. The temperature of the electron can be estimated from the slope obtained from a graph  $\text{Ln}\left(\frac{I_{ji}\lambda_{ji}}{A_{ji}g_{ji}}\right)$  versus the energy  $E_j$  (eV) a straight line has an equal slope  $\frac{1}{k_B T_e}$

**Table 1** Parameters of the spectroscopy of measured lines emitted from Pt plasma plume corresponding to the NIST database by FHG laser [12]

Wavelength	Transition		$g_k A_{ki}$	$E_k$
$\lambda$ (nm)	From	To	( $s^{-1}$ )	(eV)
530.10	$5d^8 6s(^4F)6p$	$\rightarrow 5d^8(^3F_4)6s7s(^3S_1)$	1.3e+09	6.8985567
602.60	$5d^8 6s(^4F)6p$	$\rightarrow 5d^8(^3F_4)6s7s(^3S_1)$	2.5e+08	7.0403577
630.83	$5d^9 6p$	$\rightarrow 5d^9 7s$	2.01e+08	6.5299001
665.55	$5d^8 6s(^2F)6p$	$\rightarrow 5d^9 6d$	2.e+08	7.4082005
796.36	$5d^8 6s(^4F)6p$	$\rightarrow 5d^8(^3F_4)6s7s(^1S_0)$	7.80E+01	7.5486521

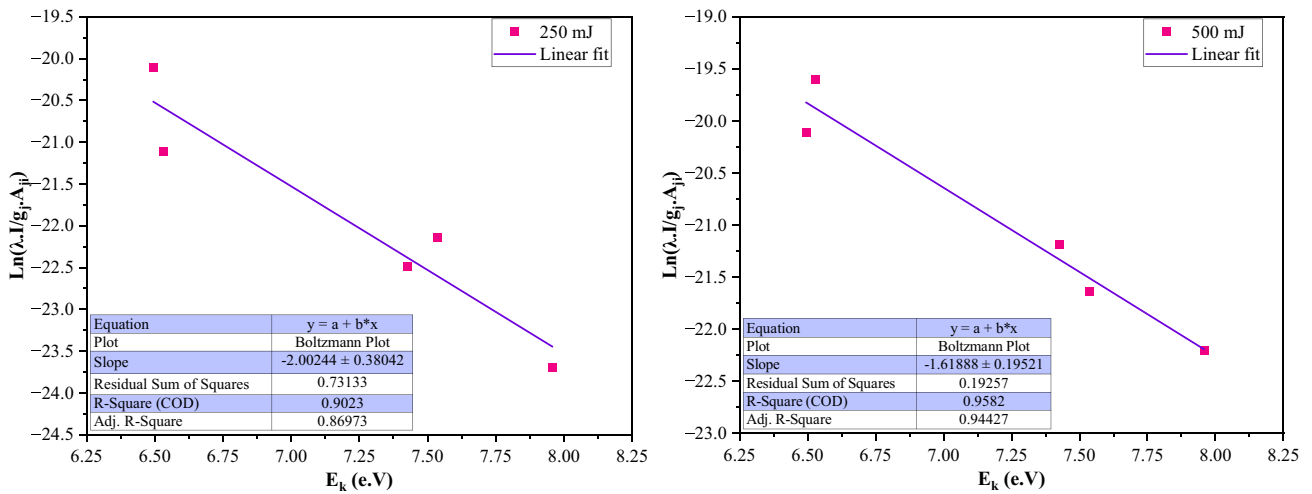


**Fig. 3** Boltzmann plot for four neutral and ion c spectral lines at laser energy range 250–500 mJ using  $\lambda = 532$  nm

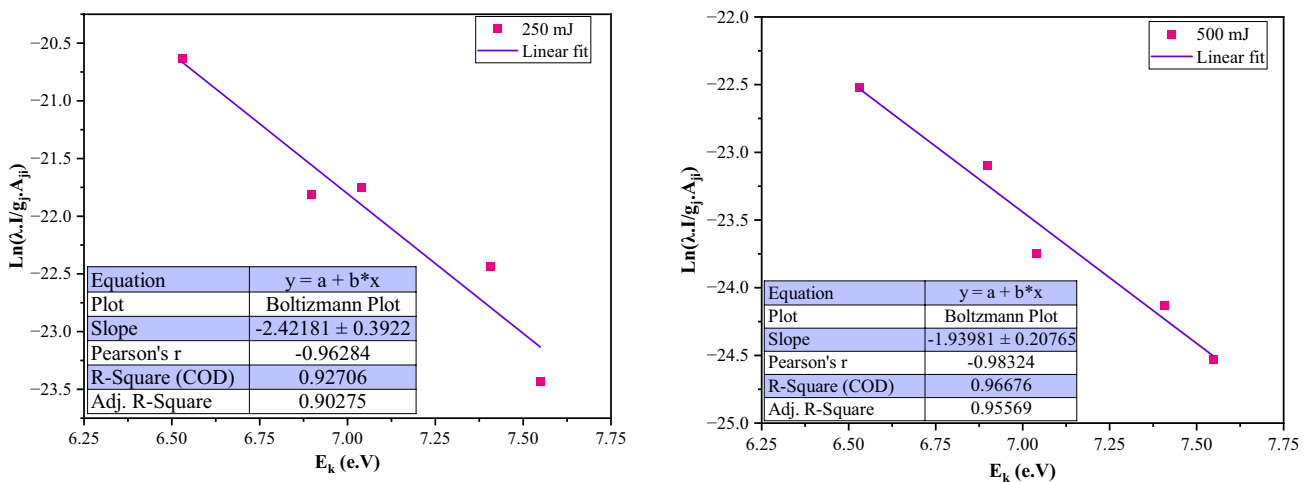


**Fig. 4** Boltzmann plot for four neutral and ion c spectral lines at laser energy range 250–500 mJ using  $\lambda = 1064$  nm

The electron temperature in Pt plasma plumes was calculated by changing the pulse laser energy to 250, and 500 mJ at both modes (1064 and 532 nm) of the Nd:YAG laser. Depending on laser pulse energy and wavelength, Pt plasma plumes' temperature values range from 0.446 to 0.62 eV, as seen in Tables 3 and 4. The electron temperature is higher as the laser energy and wavelength increase and ranges from 0.5 to 0.62 eV for the plasma caused by the  $\lambda$  1064 nm. However, we noticed that the electron temperature ranged from 0.446 to 0.516 eV when repeating the experiment using the  $\lambda$  532 nm at the same ambient conditions. It is possible to understand two reasons why the plasma plume's temperature increases with the laser pulse's energy. First, the result of an increase in the rate of mass ablation [15]. Second, one of the two possibilities of interaction is called "plasma shielding" [16]. The first reason is when the plasma is created, through electron-neutral inverse Bremsstrahlung or the electron-ion inverse Bremsstrahlung, the plasma will absorb part of the laser beam, and the second reason is through the photo-ionization-dominated interaction. Except for the early phases of the laser evaporation process, the electron-neutral process's probability is much less than that of the electron-ion processes. Thus, electron-neutral processes during laser ablation are considered negligible [17]. As shown in Table 2 from a standard spectrum of the NIST database [12]).

**Electron density**

The electron number density is a significant parameter used to describe the plasma environment, which is essential for evaluating its equilibrium (LTE) criterion. The Stark broadening line profile of an isolated single-charged ion or line neutral is one of the main methods used for estimating the electron number density ( $n_e$ ). Stark broadening is one of the dominant broadening methods in LIP, with 2–4 orders larger than other methods such as natural broadening and Doppler broadening [18]. The plasma  $n_e$  electron density is indicated by Eq. (2) for the full width at half maximum (FWHM) of the Stark broadening lines [19]:

$$\Delta\lambda_{\frac{1}{2}} = 2\omega\left(\frac{n_e}{10^{16}}\right) + 3.5A\left(\frac{n_e}{10^{16}}\right)^{\frac{5}{4}}\left[1 - \frac{3}{4}N_D^{-1/3}\right]\omega \quad (2)$$

in empirical formula (2),  $\Delta\lambda_{\frac{1}{2}}$  refers to the Stark full width at half maximum (FWHM), and  $\omega$  is the electron impact parameter, which is based on reference data, which corresponds to different electron temperatures.  $n_e$ ,  $A$ , and  $N_D$  denote the electron density, broadening ionic impact parameter, and the number of particles in the Debye sphere. The ionic broadening was neglected due to its minimal [20] contribution to the broadening: hence, Eq. (2) can then be defined in Eq. (3). The electron density  $n_e$  corresponds to the (FWHM) of the Stark broadening lines of the plasma plume [21]:

$$n_e = \left(\frac{\Delta\lambda}{2w_s}\right)N_r \quad (3)$$

Figure 5a and b illustrates the full width at half maximum (FWHM) of the Stark-broadened profile of the O I, and Pt I emission lines for 532 and 1064 nm, respectively, which may be used to calculate the Stark broadening center of 777.59, and 845.23 nm, respectively. In comparison to the practical and theoretical values that were given in the literature,  $w_s$  (0.04)  $\text{\AA}$  was utilized at a  $N_r$  equal to  $(1.00 \times 10^{17}) \text{ cm}^{-3}$  for the O I, and Pt I spectral lines, respectively.

The research findings demonstrate a direct correlation between the laser's intensity and the electron density of the plasma. Increasing the intensity of a laser leads to heightened interactions with the material it is composed of, resulting in an elevated level of ionization and electron production. Consequently, an augmentation in the laser power frequently leads to an elevation in the electron density within the plasma. The intensity of the line at 532 nm is lower compared to that of the 1064 nm laser. The laser exhibits a reduction in the number of photons by half, while simultaneously doubling the energy per photon. Furthermore, the exit energy can be reduced by going through the second harmonic crystal [22].

**Table 2** Parameters of the spectroscopy of measured lines emitted from Pt plasma plume corresponding to the NIST database by SHG laser [12]

Wave-length $\lambda$ (nm)	Transition		$g_k A_{ki}$ ( $\text{s}^{-1}$ )	$E_k$ (eV)
	From	To		
652.34	$5d^9 6p$	$\rightarrow 5d^9 7s$	2.e+08	6.5299001
705.62	$5d^8 6s(^2F)6p$	$\rightarrow 5d^8(^3F_4)6s7s$ ( $^3S_1$ )	3.0e+08	7.5370465
773.85	$5d^8 6s(^4P)6p$	$\rightarrow 5d^9 6d$	7.80e+01	7.4244726
791.12	$5d^8 6s(^4F)6p$	$\rightarrow 5d^8 6s(^4F)6p$	1.6e+08	7.9575867
820.44	$5d^8 6s(^4F)6p$	$\rightarrow 5d^9 7s$	3.0e+08	6.4942138

**Debye length  $\lambda_d$ , plasma frequency  $f_p$**

After determining the  $T_e$  in eV and  $n_e$  in  $1 \text{ cm}^{-3}$ , it is now able to compute the  $\lambda_d$  in cm using equation [23]:

$$\lambda_d = \sqrt{\frac{\epsilon_0 K_B T_e}{e^2 n_e}} \quad (4)$$

if we express the preceding equation as [23], where  $\epsilon_0$  represents the permittivity of the vacuum,  $K_B$  stands for the Boltzmann constant, and  $e$  stands for the charge of an electron, then we have:

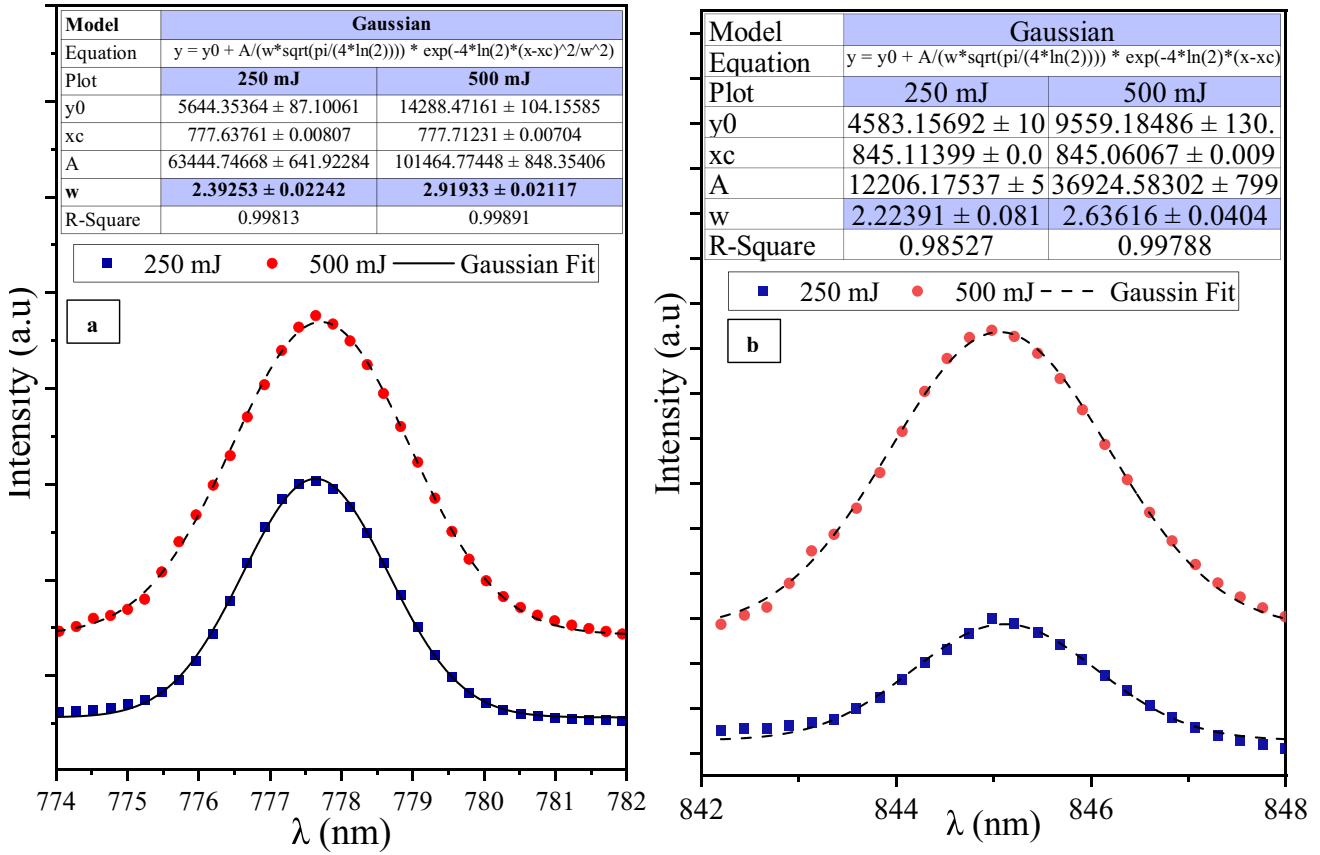


Fig.5 Gaussian fitting of the a O (I) for 532 nm and b (Pt I) for 1064 nm transition for a variety of energies

Table 3 Plasma parameters from Pt plasma plume by first harmonic generation laser

E (mJ)	T <sub>e</sub> (eV)	FWHM (nm)	w <sub>s</sub> (nm)	N <sub>r</sub> × 10 <sup>17</sup> (cm <sup>-3</sup> )	N <sub>e</sub> × 10 <sup>16</sup> (cm <sup>-3</sup> )	λ <sub>D</sub> × 10 <sup>-5</sup> (cm)	f <sub>p</sub> × 10 <sup>12</sup> (Hz)	N <sub>D</sub> particle
250	0.50	2.392	4.30	1.00	2.78	3.15	1.50	3636.87
500	0.62	2.929	4.30	1.00	3.41	3.17	1.66E	4523.52

Table 4 Plasma Parameters from Pt plasma plume by Second harmonic generation laser

E (mJ)	T <sub>e</sub> (eV)	FWHM (nm)	w <sub>s</sub> (nm)	N <sub>r</sub> × 10 <sup>17</sup> (cm <sup>-3</sup> )	N <sub>e</sub> × 10 <sup>16</sup> (cm <sup>-3</sup> )	λ <sub>D</sub> × 10 <sup>-5</sup> (cm)	f <sub>p</sub> × 10 <sup>12</sup> (Hz)	N <sub>D</sub> particle
250	0.446	2.221	4.30	1.00	2.58	3.09	1.44	3184.33
500	0.516	2.636	4.30	1.00	3.07	3.05	1.57	3634.67

$$\lambda_d = 7430 \left( \frac{T}{n_e} \right)^{\frac{1}{2}} \text{ (cm)} \tag{5}$$

the frequency of plasmas may be described as follows [4]:

$$f_p = \frac{n_e e^2}{m_e \epsilon_0} \tag{6}$$

where  $f_p$  is the frequency of the plasmas that is an extremely important aspect, and the electron mass is denoted by  $m_e$

To get the Debye number, another option is to apply the following equation:

$$N_D = \frac{4}{3} \pi n_e \lambda_D^3 = 1.38 \times 10^6 T^{3/2} n_e^{1/2} \tag{7}$$

The pulse's intensity causes the plasma's electrons to heat up. This is consistent with previous research for other elements that showed raising the strength of pulses raised both  $T_e$  and  $n_e$  in the platinum plasmas. Tables 3 and 4 numbers back up this claim. We note that as the laser pulse energy increases, the Debye length ( $\lambda_D$ ) decreases; this is because lasers can have different effects on plasma, depending on their intensity and frequency. However, in general, increasing the energy of the laser pulse increases the temperature ( $T_e$ ) of the material by an amount sufficient to separate the outermost electron from the atom, and thus leads to a significant increase in electron density.

The increase in electron temperature found when using a primary laser with a longer wavelength compared to a second harmonic laser can be attributed to several factors, such as differences in laser–plasma interactions, energy absorption, or heating mechanisms. To determine the exact cause, a thorough investigation of the experimental setup, the interactions between the laser and plasma, and the underlying physics mechanisms would be necessary. It is postulated that the interaction between the plasma and the laser with longer wavelengths may result in an augmented transfer of energy to the electrons. The potential correlation between the rise in electron temperature and the utilization of a primary laser with a longer wavelength could be attributed to variances in energy deposition and absorption mechanisms. Wavelengths of greater length possess the ability to penetrate the plasma to a greater extent, so engaging with a bigger quantity of particles facilitates the transfer of a greater amount of energy to the electrons. The increased energy absorption observed in this scenario may result in elevated electron temperatures in comparison to the second harmonic laser with a lower wavelength, which may exhibit limited penetration into the plasma.

## Conclusion

The research on spectroscopic diagnostics of plasma generated from a pure platinum target using the optical emission method provides useful insights into the properties and behavior of the plasma under investigation. By utilizing spectroscopic techniques, one may conduct a thorough analysis of the light emitted, which allows for a detailed understanding of the plasma's elemental composition, temperature, and other relevant characteristics. The results obtained from this work improve our understanding of plasma dynamics and provide essential information for potential applications in various fields, such as materials science, plasma technology, and spectroscopy. A crucial stage in research and development is the identification and quantification of the spectral lines that are present in the emitted light spectrum. This technique can make significant advancements

in plasma diagnostics and related technologies. Moreover, the outcomes may have implications for improving plasma-based techniques that employ pure platinum targets, such as plasma-assisted material deposition, surface modification, or analytical applications. Gaining knowledge from this work enhances our ability to control and manipulate plasmas for specific purposes, fostering progress in both scientific and technical domains.

**Acknowledgements** We thank the Medical Physics Lab., Department of Physics, and College of Science for Women, University of Baghdad

## References

1. SN Mazhir NA Abdullah HI Al-Ahmed NH Harb NK Abdalameer The effect of gas flow on plasma parameters induced by microwave Baghdad Sci. J. 15 2 0205 0205, (2018) <https://doi.org/10.21123/bsj.2018.15.2.0205>
2. E Mazalan K Chaudhary Z Haider SF Abd Hadi J Ali Determination of calcium to phosphate elemental ratio in natural hydroxyapatite using LIBS J. Phys. Conf. Ser. 1027 1 1 8 (2018) <https://doi.org/10.1088/1742-6596/1027/1/012013>
3. RH Jassim NK Abdalameer EK Jebur Applications in biomedicine and fabrication using plasma and nanomaterials Int. J. Nanosci. 22 6 2330003, (2023)
4. M Hanif M Salik F Arif Spectroscopic study of carbon plasma produced by the first (1064 nm) and second (532 nm) harmonics of Nd: YAG laser Plasma Phys. Rep 41 3 274 280, (2015) <https://doi.org/10.1134/S1063780X15030034>
5. WH Chiang D Mariotti RM Sankaran JG Eden K Ostrikov Microplasmas for advanced materials and devices Adv. Mater. 32 18 1905508, (2020) <https://doi.org/10.1002/adma.201905508>
6. AN Yasoob NK Abdalameer AQ Mohammed Plasma production and applications: a review Int. J. Nanosci. 21 06 2230003, (2022)
7. G Murtaza NM Shaikh GA Kandhro M Ashraf Laser induced breakdown optical emission spectroscopic study of silicon plasma Spectrochim. Acta Part A Mol. Biomol. Spectrosc. 223 117374, (2019) <https://doi.org/10.1016/j.saa.2019.117374>
8. H Yao Investigation into the effect of increasing target temperature and the size of cavity confinements on laser-induced plasmas Metals (Basel) 10 30 393, (2020)
9. HH Murbat NKH Abdalameer AK Brrd F Abdulameer Effects of non-thermal argon plasma produced at atmospheric pressure on the optical properties of CdO thin films Baghdad Sci. J. 15 2 0221, (2018) <https://doi.org/10.21123/bsj.2018.15.2.0221>
10. NK Abdalameer RH Jassim EK Jebur SN Mazhir Laser pulse's frequency effect on plasma parameters for titanium dioxide produced by FHG of a Q-switched ND: YAG pulse laser Int. J. Nanosci. 22 02 2350011, (2023)
11. HH Abbas SN Mazhir NK Abdalameer Calculate of plasma parameters produce from copper target using Boltzmann-plots method Int. J. Nanosci. 22 5 2350042 138, (2023)
12. National Institute of Standards and Technology (NIST) atomic spectra database (version 5), [https://physics.nist.gov/PhysRefData/ASD/lines\\_form.html](https://physics.nist.gov/PhysRefData/ASD/lines_form.html)
13. F Ruan T Zhang H Li Laser-induced breakdown spectroscopy in archeological science: a review of its application and future perspectives Appl. Spectrosc. Rev. 54 7 573 601, (2019) <https://doi.org/10.1080/05704928.2018.1491857>
14. M Hanif M Salik MA Baig Diagnostic study of nickel plasma produced by fundamental (1064 nm) and second harmonics (532 nm)

- of an Nd: YAG laser J. mod. Phy. 3 10 1663, (2012) <https://doi.org/10.4236/jmp.2012.330203>
15. F Anabitarte A Cobo Laser-Induced breakdown spectroscopy: fundamentals, applications, and challenges ISRN Spectrosc. 285240 12, (2012) <https://doi.org/10.5402/2012/285240>
  16. M Hanif M Salik MA Baig Quantitative studies of copper plasma using laser-induced breakdown spectroscopy Opt. Lasers Eng. 49 12 1456 1461, (2011) <https://doi.org/10.1016/j.optlaseng.2011.06.013>
  17. SU Haq L Ahmat M Mumtaz H Shakeel S Mahmood A Nadeem Spectroscopic studies of magnesium plasma produced by fundamental and second harmonics of Nd: YAG laser spectroscopic studies of magnesium plasma produced by fundamental and second harmonics of Nd: YAG laser Phys. Plasmas 22 083504 1 8, (2015) <https://doi.org/10.1063/1.4928376>
  18. KA Aadim SN Mazhir NK Abdalameer AH Ali Influence of gas flow rate on plasma parameters produced by a plasma jet and its spectroscopic diagnosis using the OES technique IOP Conf. Ser. Mater. Sci. Eng. 28 987 01, (2020) <https://doi.org/10.1088/1757-899X/987/1/012020>
  19. E Mazalan K Chaudhary Z Haider SF Abd Hadi J Ali Determination of calcium to phosphate elemental ratio in natural hydroxyapatite using LIBS J. Phys. Conf. Ser. 1027 1 1 8, (2018) <https://doi.org/10.1088/1742-6596/1027/1/012013>
  20. AS Noori NK Abdalameer SN Mazhir MK Mohammed Investigation of the plasma parameters induced from a silver source in air using Boltzmann-Blott approach Int. J. Mod. Phy. B 37 10 1 10, (2023) <https://doi.org/10.1142/S021797922350100X>
  21. E Asamoah Y Xia Y Hongbing P Wei C Jiawei Influence of cavity and magnetic confinements on the signal enhancement and plasma parameters of laser-induced Mg and Ti plasmas Laser Part. Beams 38 1 1 12, (2020) <https://doi.org/10.1017/S0263034620000014>
  22. M Ruthandi Y Okamoto K Hamada A Okada S Nakashima N Nishi Effects of superposition of 532 nm and 1064 nm wavelengths in copper micro-welding by pulsed Nd: YAG laser J. Mater. Process. Tech. 299 11 13, (2023) <https://doi.org/10.1016/j.jmatprotec.2021.117388>
  23. NK Abdalameer SN Mazhir KA Aadim Diagnostics of zinc selenite plasma produced by FHG of a Q-switched Nd: YAG laser Chalcogenide Lett. 18 7 405 411, (2021)

**Publisher's Note** Springer Nature remains neutral with regard to jurisdictional claims in published maps and institutional affiliations.

Springer Nature or its licensor (e.g. a society or other partner) holds exclusive rights to this article under a publishing agreement with the author(s) or other rightsholder(s); author self-archiving of the accepted manuscript version of this article is solely governed by the terms of such publishing agreement and applicable law.